Acousto–defect interaction in irradiated and non–irradiated silicon n^+–p–structure

O. Ya. Olikh,[1, a)] A. M. Gorb,[1] R. G. Chupryna,[1] and O. V. Pristay–Fenenkov[1]

Faculty of Physics, Taras Shevchenko National University of Kyiv, Kyiv 01601,
Ukraine

The experimental investigation of ultrasound influence on the electrical characteristics of silicon n^+–p–structure has been carried out. The effects of reactor neutrons and ^{60}Co gamma radiation on ultrasound influence were studied. It has been found out that the ultrasound loading leads to reversible change of shunt resistance, carrier lifetime in both space charge and quasi–neutral regions, ideality factor. Acoustically induced alteration of last two parameters depends on irradiation considerably. The models of coupled defect level recombination, Shockley–Read–Hall recombination, and dislocation–induced impedance were used to describe findings. It has been shown that the observed phenomena can deal with the increase of distance between coupled defects as well as an extension of carrier capture coefficient of complex point defect and dislocation. It has been shown that divacancy and pair vacancy–interstitial oxygen are effectively modified by ultrasound in contrast to complex interstitial carbon–interstitial oxygen.

Keywords: acousto–defect interaction, silicon, irradiation

I. INTRODUCTION

It has been shown experimentally that ultrasound (US) can effectively interact with defects. US as defect engineering tool has some advantages: (i) locality of the action due to the predominant absorption in regions of deviation in the lattice periodicity; (ii) selectivity of the influence, which is achieved by variation of acoustic wave (AW) polarization and type; (iii) possibility of resonance transformation in the defect system due to the oscillation nature of action; (iv) capability of reversible effect in the case of low intensity AW.

In the case of piezoelectric semiconductors, the acousto–defect interaction (ADI) is determined mainly by electric field, which accompanies the vibration wave propagation. This effect is expected and something related to acousto–electric phenomena. But US influence on defect system is also observed in non–piezoelectric crystals like silicon, which is microelectronic dominant material. Thus it was experimentally observed in silicon structures, that US caused an atomic diffusion,[1,2] transformed a native and an impurity defect,[3–7] modified interior surface states,[8–10] created new defect.[11,12] Defects are known to determine a most of semiconductor device properties. And exactly the ADI is a reason of variation of a tunneling,[13,14] a generation–recombination[15–17] and a thermionic emission[18,19] current in silicon barrier structures.

The main mechanisms of elastic vibration–defect interaction in non-piezoelectric crystals are considered to be the change of population of impurity oscillator levels,[20] the displacement of impurity atoms with respect to their surroundings,[4,21,22] the decreasing of the diffusion activation energy,[23] the local temperature increase by point

defect clusters,[24] the US absorption by dislocation.[16,25,26] However to the best of our knowledge, the complete ADI theory in silicon is absent. One of a top–ranked cause is a lack of experimental works, which have focused on investigation of acoustically induced (AI) effects.

Not all silicon defects are acoustically active and subjected to modification under US action. The ADI efficiency depends on the defect type and structure.[8] Thus, the force acting on the point defect during US loading (USL) is determined by the relaxation of the defect volume[21,22]. The irradiation is most widespread and studied method of semiconductor defects alteration. On the one hand, the high–power US treatment is shown[27–30] to lead to residual changes of the irradiated silicon structure properties. This effect deals with AI annealing of radiation defects (RDs). On the other hand, irradiation can be a reason of reversible AI phenomenon initiation,[31,32] which is caused by formation of acoustically active RDs. Unfortunately, there have only a few reports on acoustically driven phenomenon in irradiated silicon structures.

Our goal is to investigate experimentally the AI electrical characteristic variation, which takes place in non–irradiated and irradiated n^+–p–Si structures. Irradiation was carried by reactor neutrons and a ^{60}Co–gamma source. It is expected that γ–rays introduce VO$_i$ complex predominantly,[33–35] whereas neutrons create vacancy clusters,[36,37] disordered regions[38] and C$_i$O$_i$ complex[35,39] mainly. This work represents distinction of AI effects in silicon structures with different RDs. The used US intensity was not very high to avoid the irreversible defect subsystem modification, which can deal with a new defect creation, a RDs annealing or a long distance (a many interatomic distance) diffusion. As a result, the characteristic full recovery was observed after the stop of an AW propagation. The models of coupled defect level recombination,[40,41] Shockley–Read–Hall (SRH) recombination, and dislocation–induced impedance[42,43] were

a)Electronic mail: olikh@univ.kiev.ua

TABLE I. The sample irradiation parameters.

Sample	Irradiation type	D (rad)	Ψ (cm^{-2})	NIEL[a] (MeV cm^2/g)	$\Psi \times$NIEL (MeV/g)
iSC	non	0	0	—	0
nSC	neutron	$4.5 \cdot 10^3$	$4 \cdot 10^{11}$	$2.04 \cdot 10^{-3}$	$8.2 \cdot 10^8$
g6SC	γ–^{60}Co	$1 \cdot 10^6$	$1.6 \cdot 10^{15}$	$1.07 \cdot 10^{-7}$	$1.7 \cdot 10^8$
g7SC	γ–^{60}Co	$1 \cdot 10^7$	$1.6 \cdot 10^{16}$	$1.07 \cdot 10^{-7}$	$1.7 \cdot 10^9$

[a] Ref. 44.

TABLE II. The ultrasound loading parameters.

Sample	W_{US} (W/cm^2)	ξ_{US} (10^{-6})	u_{US} (nm)	USL label
iSC	0.22	3.1	0.67	Ui–1
	0.40	4.2	0.91	Ui–2
nSC	0.24	3.2	0.70	Un–1
	0.40	4.2	0.91	Un–2
g6SC	0.38	4.1	0.89	Ug6–2
g7SC	0.19	2.9	0.63	Ug7–1
	0.37	4.0	0.87	Ug7–2

used to describe the processes in the space charge region (SCR), in the diode base, and shunt resistance, respectively. The interaction of defects with an AW strain field[21,22] was recruited to explain the observed AI phenomena. The investigation would provide not only better ADI understanding but could also facilitate the development of acoustically controlled devices or radiation sensors.

II. EXPERIMENTAL AND CALCULATION DETAILS

The 2 inch (300 μm thick) p–type boron doped, <111> orientation, Czochralski silicon wafer having resistivity of 10 Ω·cm was used for fabrication of n$^+$–p–Si structure. The n$^+$ emitter with carrier concentration of about 10^{19} cm^{-3} and thickness of 0.5 μm was formed by phosphorus implantation. Aluminium front and rear electrodes were deposited by screen printing before rapid annealing. Samples with area of about 2 cm^2 were cut from the central part of the wafer and used in experiment. Samples were irradiated by reactor neutrons or by ^{60}Co γ–rays. Doses D, fluences Ψ, and sample labels are listed in Table I. Data[44,45] were used to determine D and Ψ correlation. The non–ionizing energy losses (NIEL) for neutron and γ–^{60}Co are shown in Table I too. As displacement damage effect is characterized by ($\Psi \cdot$ NIEL), the similar damage is expected in investigated samples. To avoid an impact of long–term annealing, which is typical to neutron damaged structure especially,[35,36] irradiated samples have been stored for 5 years at room temperature before measuring.

The dark forward current–voltage (I–V) characteristics of the samples both with and without USL were measured over a temperature range 290–340 K. The temperature was controlled by differential copper–constantan thermocouple. Some curves are shown in Fig. 1.

The double–diode model of n$^+$–p structure I–V characteristic is expressed in the following form:

$$I(V, T) = I_{SCR} + I_{base} + I_{sh} , \quad (1)$$

$$I_{SCR} = \frac{qAn_i d}{2\tau_g} \left\{ \exp\left[\frac{q(V - IR_s)}{n_{id}kT}\right] - 1 \right\} , \quad (2)$$

$$I_{base} = \frac{qAn_i^2}{p_p} \sqrt{\frac{\mu_n kT}{\tau_n}} \left\{ \exp\left[\frac{q(V - IR_s)}{kT}\right] - 1 \right\} , (3)$$

$$I_{sh} = (V - IR_s)/R_{sh} , \quad (4)$$

where I_{SCR} reflects the overall SCR recombination, I_{base} is closely related to recombination in the quasi–neutral region, I_{sh} is the shunt current, A is the sample area, n_i is the intrinsic carrier concentration, τ_g is the SCR carrier lifetime, d is the SCR thickness:

$$d = \sqrt{\frac{2\varepsilon\varepsilon_0}{qp_p}\left[\frac{E_g}{q} - \frac{kT}{q}\ln\left(\frac{N_v N_c}{p_p n_n}\right) - \frac{2kT}{q} - V\right]}, \quad (5)$$

ε is the permittivity (11.7 for Si), p_p and n_n are the majority carrier concentration in the p– and n–type regions, E_g is the semiconductor band gap, N_c and N_v are the effective density of states in the conduction and valence bands; n_{id} is the ideality factor, R_s and R_{sh} are the series and shunt resistances, μ_n and τ_n are the electron (minority carrier) mobility and lifetime in the diode base.

We used Eqs. (1)–(5) to fit the experimental data and τ_g, τ_n, n_{id}, R_{sh}, and R_s were taken as the fittings parameters. The known[46–48] temperature dependencies of n_i, E_g, and μ_n were used. The extremely good fit to the experimental data was obtained — see Fig. 1. In particular, the R_s value about 1 Ω was determined for all samples.

In the USL case, the transverse AWs with frequency of 4.2 MHz were exited with help of a piezoelectric transducer and were injected in samples from the base side in the [111]–direction. The US intensities W_{US}, amplitudes of lattice deformation ξ_{US} and lattice atom displacement u_{US} are listed in Table II. It was reported previously[6,7,19] that the characteristic time of change in the silicon structure parameters under the US action did not exceed $2 \cdot 10^3$ s. In order to wait till the AI transitional period the following experimental procedure has been used. After USL start the sample has been kept at room temperature during 60 min and then the I–V measurement and the sample heating were started. In order to avoid the effect of piezoelectric field on I–V characteristics, the piezoelectric transducer has been shielded.

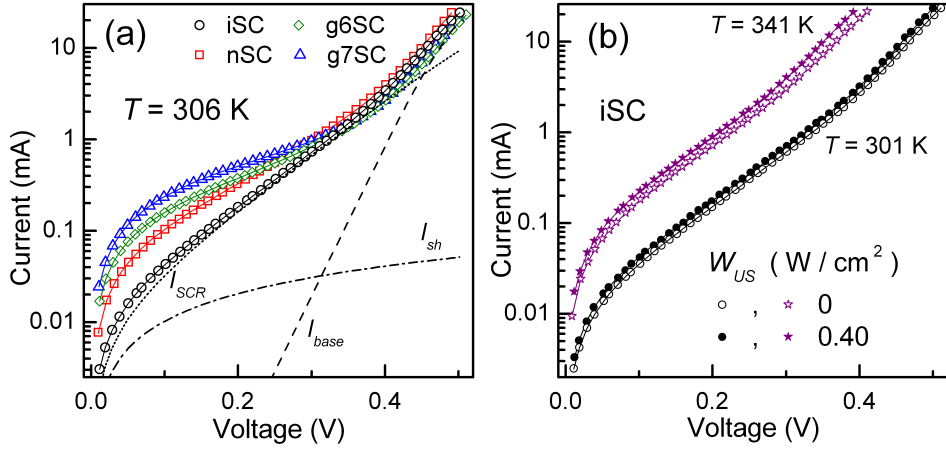The non-linear fittings were done by using the differential evolution method.[49]

FIG. 1. Dark I–V characteristics measured (a) at 306 K for non–irradiated (circles), neutron–irradiated (squares) and gamma–irradiated (diamonds and triangles) structures without USL; (b) at 301 K (circles) and 341 K (asterisks) with (filled marks, Ui–2) and without (open marks) USL for the iSC. The marks are the experimental results, the solid lines are the fitted curves using Eqs. (1)–(5). The dashed, dot–dashed and dotted lines in (a) are the base, SCR and shunt components of iSC current, respectively.

III. RESULTS AND DISCUSSION

A. Space charge region

The I–V characteristic parameters, which deal with SCR phenomena, are n_{id} and τ_g. The finding temperature dependences of ideality factor and SCR carrier lifetime are shown in Fig. 2 and Fig. 3, respectively.

As one can recognize, ideality factor decreases with temperature increase and the plot n_{id} vs $1/T$ is close to linear. Thus dependence $n_{id}(T)$ can be expressed as

$$n_{id}(T) = n_{id,\infty} + T_{id}/T \ . \tag{6}$$

The thermoactivated growth of SCR lifetime is observed over the explored temperature range — see Fig. 3. The following equation allows to describe sufficiently τ_g temperature dependence:

$$\tau_g(T) = \tau_{g0} \exp\left(-\frac{E_{\tau g}}{kT}\right) \ . \tag{7}$$

The T_{id} and $E_{\tau g}$ values, which have been determined for both non-irradiated and irradiated samples with as well as without USL are listed in Table III.

We want to stress, that
(i) irradiation leads to T_{id} and $E_{\tau g}$ changes, the g6SC's ideality factor characteristic temperature and SCR lifetime characteristic energy values are closely related to g7SC ones at similar conditions;
(ii) USL affects n_{id} and τ_g values, absolute AI changes of ideality factor $\Delta n_{id} = n_{id,US} - n_{id,in}$ and relative AI changes of SCR lifetime $\varepsilon_{\tau g} = (\tau_{g,US} - \tau_{g,in})/\tau_{g,in}$ (where subscripts "US" and "in" identify with values, which are obtained at the same temperature with and without USL respectively) are listed in Table IV;

(iii) Δn_{id} and $\varepsilon_{\tau g}$ vary with W_{US} enhancement, whereas T_{id} and $E_{\tau g}$ values do not depend on US intensity practically.
(iv) USL results in both T_{id} and $E_{\tau g}$ increase in γ–irradiated samples — see Fig. 2(b) and Fig. 3(b), but same effect is not observed in non–irradiated and neutron–irradiated samples — see Fig. 2(a) and Fig. 3(a);
(v) Δn_{id} and $\varepsilon_{\tau g}$ have an opposite sign for non–irradiated and irradiated samples (for SCg6 not in whole temperature range);
(vi) ideality factor is varied by USL more effectively in irradiated samples;

For purpose of the present consideration, it is important to discuss the recombination mechanism in the SCR of the investigated samples. According to classical SRH theory, an ideality factor must be less than 2 and τ_g temperature dependence is expected[50,51] to be described by the relation $\tau_g \simeq 2\tau_n \sqrt{\sigma_n/\sigma_p} \cosh\left[(E_t - E_i)/kT\right]$ (where σ_n, σ_p, and E_t are the electron and hole capture cross sections (CCSs) and the energy level of the recombination center, E_i is the intrinsic energy level). In the our case, n_{id} is lager than 2 and τ_g increases with temperature. Therefore SRH theory is inapplicable to the investigated samples. Several attempts to explain large n_{id} have been made with various models.[52–55] But all observed features of SCR recombination (ideality factor large value, independence on light intensity, dependence on temperature as well as carrier lifetime small value) can be explained by the model of coupled defect level recombination (CDLR)[40,41] only. This model provides a rapid direct charge transfer between defect levels. Such phenomenon has been observed experimentally firstly[56,57] and then it was recruited to explain process in semiconductor diodes.[40,41,58]

According to the CDLR model, recombination is the result of carrier exchange between two defect level and
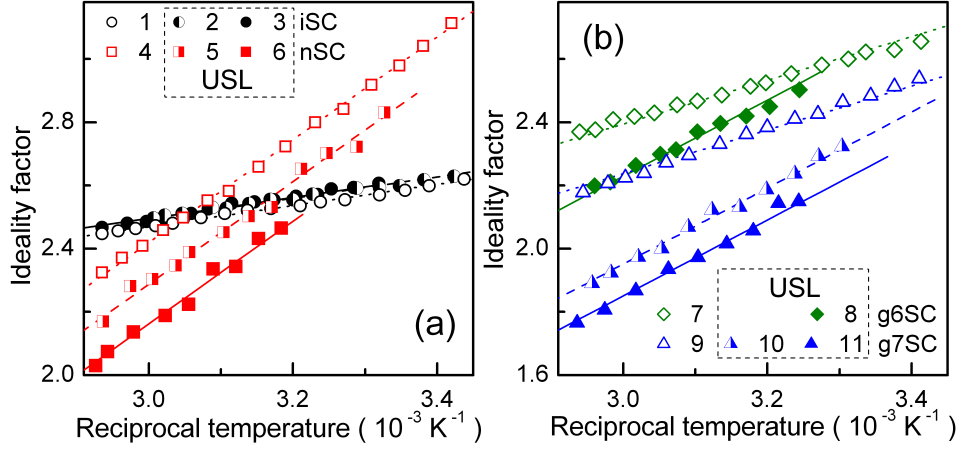
FIG. 2. Temperature dependences of ideality factor for non–irradiated (curves 1–3, circles), neutron–irradiated (4–6, squares) and γ–irradiated (7–11, diamonds and triangles) samples. The curves 1, 4, 7 and 9 (open marks) are obtained without USL, curves 2, 3, 5, 6, 8, 10, and 11 correspond to Ui–1, Ui–2, Un–1, Un–2, Ug6–2, Ug7–1, and Ug7–2 respectively. The marks are the experimental results, the lines are the fitted curves using Eq. (6).
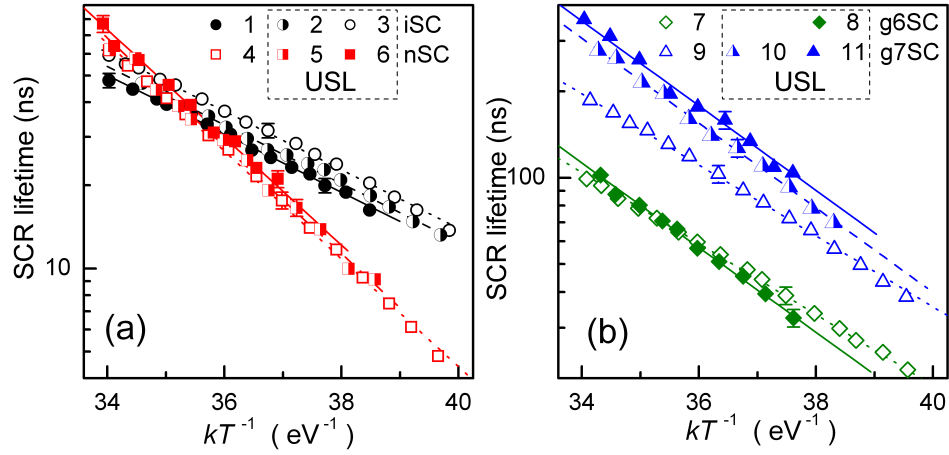

FIG. 3. Temperature dependences of SCR lifetime for non–irradiated (curves 1–3, circles), neutron–irradiated (4–6, squares) and γ–irradiated (7–11, diamonds and triangles) samples. The curves 1, 4, 7 and 9 (open marks) are obtained without USL, curves 2, 3, 5, 6, 8, 10, and 11 correspond to Ui–1, Ui–2, Un–1, Un–2, Ug6–2, Ug7–1, and Ug7–2 respectively. The marks are the experimental results, the lines are the fitted curves using Eq. (7).

TABLE III. Characteristics of temperature dependences of n^+–p–Si structure parameters.

Sample	USL	T_{id} (K)	$E_{\tau g}$ (eV)	$R_{293,\mathrm{Al}}$ (kΩ)	σ_{dis} (10^4 K/Ω)
iSC	non	330 ± 30	0.24 ± 0.01	27 ± 3	41 ± 4
	Ui–1	310 ± 30	0.24 ± 0.01	27 ± 3	50 ± 4
	Ui–2	360 ± 30	0.24 ± 0.01	26 ± 3	58 ± 4
nSC	non	1610 ± 70	0.45 ± 0.02	2.2 ± 0.4	65 ± 7
	Un–1	1600 ± 70	0.44 ± 0.02	2.3 ± 0.4	95 ± 10
	Un–2	1680 ± 70	0.44 ± 0.02	2.2 ± 0.4	130 ± 10
g6SC	non	610 ± 40	0.28 ± 0.01	0.7 ± 0.1	19 ± 2
	Ug6–2	1080 ± 50	0.33 ± 0.02	0.8 ± 0.1	24 ± 2
g7SC	non	770 ± 50	0.29 ± 0.01	0.41 ± 0.06	26 ± 3
	Ug7–1	1260 ± 60	0.34 ± 0.02	0.39 ± 0.06	45 ± 4
	Ug7–2	1270 ± 60	0.35 ± 0.02	0.38 ± 0.06	55 ± 4

TABLE IV. Acoustically induced change of n^+-p–Si structure parameters (at 330 K).

Sample	USL	Δn_{id} (±0.01)	$\varepsilon_{\tau g}$ ($\pm5\%$)	$\varepsilon_{\tau n}$ (±0.2)	$\varepsilon_{\sigma \mathrm{dis}}$ ($\pm10\%$)
iSC	Ui–1	0.02	-14	0.7	20
	Ui–2	0.03	-17	1.4	40
nSC	Un–1	-0.13	5	1.5	50
	Un–2	-0.26	13	3.0	100
g6SC	Ug6–2	-0.15	2	2.3	30
g7SC	Ug7–1	-0.26	49	0.9	70
	Ug7–2	-0.36	70	1.9	110

crystal bands. In particular, it is proposed[41] that the recombination rate is dominated by sites where an acceptor–like defect is coupled to a donor-like defect. In the simplified case of no carrier exchange between the donor level E_t^{D} and the valence band as well as between the acceptor level E_t^{A} and the conduction band, the recombination rate R can be expressed[40] as

$$R = \frac{R_{12} - \sqrt{R_{12}^2 - 4\tau_n^{\mathrm{D}}\tau_p^{\mathrm{A}}(np-n_i^2)(1-\epsilon)}}{2\tau_n^{\mathrm{D}}\tau_p^{\mathrm{A}}(1-\epsilon)}, \quad (8)$$

$$R_{12} = \frac{(n+n_{\mathrm{D}})(p+p_{\mathrm{A}})}{R_{\mathrm{DA}}} + \tau_n^{\mathrm{D}}(p+p_{\mathrm{D}}) + \tau_p^{\mathrm{A}}(n+n_{\mathrm{A}}), (9)$$

$$\tau_n^{\mathrm{D}} = (N_{\mathrm{D}}\,\sigma_n^{\mathrm{D}}\,\upsilon_{\mathrm{th},n})^{-1}, \quad \tau_p^{\mathrm{A}} = (N_{\mathrm{A}}\,\sigma_p^{\mathrm{A}}\,\upsilon_{\mathrm{th},p})^{-1}, \quad (10)$$

where R_{DA} is the coupling parameter, N_{D} and N_{A} are the density of the donor and acceptor–like defects, σ_n^{D} and σ_p^{A} are electron CCS of donor and hole CCS of acceptor, $\upsilon_{\mathrm{th},n}$ and $\upsilon_{\mathrm{th},p}$ are the thermal electron and hole velocity, $n_{\mathrm{D,A}}$, $p_{\mathrm{D,A}}$, and ϵ depend on E_t^{D}, E_t^{A}, and level degeneracy factors. As $\tau_g \propto R^{-1}$, last ones are expected to provide a thermoactivated SCR lifetime behavior. Unfortunately, the functional relation between I–V characteristic parameters and attributes of defects, which take part in CDLR, is not suggested.

According to Steingrube et al.[41], SSC for defect in a pair differs from that for isolated defect and depends on the distance between donor and acceptor r:

$$\sigma_{n,p}^{\mathrm{D,A}}(r) = C_{n,p}^{\mathrm{D,A}}\,r^2, \quad (11)$$

where C_n^{D} and C_p^{A} are some constant. Besides, R_{DA} is proportional to the overlap integral of the wave functions. If both defects are characterized by H–like radial–symmetric wave function and equal Bohr radius a_0, the following expression can be used:[41]

$$R_{\mathrm{DA}}(r) \propto N_{\mathrm{D}}N_{\mathrm{A}}\left[1 + \frac{r}{a_0} + \frac{1}{3}\left(\frac{r}{a_0}\right)^2\right]e^{-r/a_0}. \quad (12)$$

In our opinion, the observed reversible AI n_{id} and τ_g modifications are induced by donor–acceptor distance alteration in samples under USL. Really, according to data,[21,22] the force acting on the point defect during USL
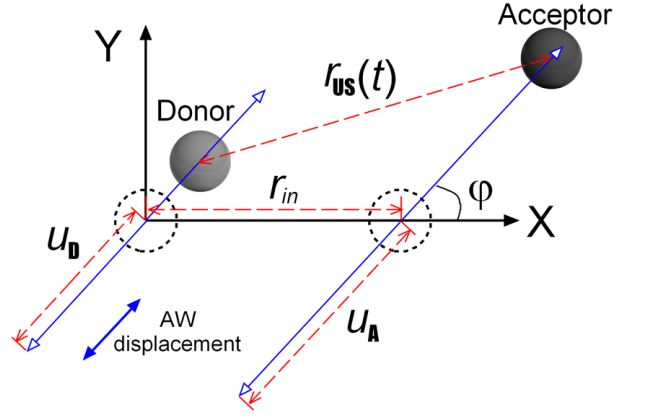

FIG. 4. Model of CDLR center behavior under US action.

can be expressed as

$$F_d = \chi\,\Delta\Omega_d\frac{\partial\xi(z,t)}{\partial z}, \quad (13)$$

where χ is the bulk elasticity modulus, $\Delta\Omega_d$ is the crystal volume change per defect, ξ is the crystal lattice deformation, and AW propagates along z direction. $\partial\xi(z,t)/\partial z \propto \xi_{\mathrm{US}}$. For interstitial atoms and substitutional impurities with the ionic radius exceeding the ionic radius of matrix atoms, the $\Delta\Omega_d > 0$, whereas, for vacancies and substitutional impurities with ionic radius smaller than the ionic radius of matrix atoms, $\Delta\Omega_d < 0$. Therefore, a point defect vibrates under USL condition and oscillation amplitude and phase are determined by both defect character and AW intensity.

Some qualitative conclusion can be drawn from the simplest model, which is shown in Fig. 4. Initially donor and acceptor are situated at distance r_{in}. Axis X is drawn through point defect inial positions. During USL defects would vibrate with amplitudes u_{D} and u_{A}. Vibration axis coincides with AW displacement direction and forms angle φ with X–axis. The amplitudes depend on ξ_{US}, defect elastic strain ($\Delta\Omega_d^{\mathrm{D}}$ and $\Delta\Omega_d^{\mathrm{A}}$), defect coupling and can be different. According to suggested model, the donor–acceptor distance in the sample with USL r_{US} depends on time t:

$$r_{\mathrm{US}}(t) = \left\{[r_{in} + u_{\mathrm{A}}\cos(\omega_{\mathrm{US}}t+\delta) - u_{\mathrm{D}}\cos(\omega_{\mathrm{US}}t)]^2\cos^2\varphi\right.$$
$$\left.+[u_{\mathrm{A}}\cos(\omega_{\mathrm{US}}t+\delta) - u_{\mathrm{D}}\cos(\omega_{\mathrm{US}}t)]^2\sin^2\varphi\right\}^{0.5}, \quad (14)$$

where ω_{US} is the US cyclic frequency, δ is the phase shift between donor and acceptor vibration.

We use Eqs. (11)–(12) to estimate AI relative changes of CCS $\varepsilon_\sigma = [\sigma_{\mathrm{US}} - \sigma(r_{in})]/\sigma(r_{in})$ and coupling parameters $\varepsilon_{\mathrm{RDA}} = [R_{\mathrm{DA,US}} - R_{\mathrm{DA}}(r_{in})]/R_{\mathrm{DA}}(r_{in})$, where σ_{US} and $R_{\mathrm{DA,US}}$ are averaged over the AW period T_{US}:

$$\sigma_{\mathrm{US}} = \frac{1}{T_{\mathrm{US}}}\int_0^{T_{\mathrm{US}}}\sigma(r_{\mathrm{US}}(t))dt, R_{\mathrm{DA,US}} = \frac{1}{T_{\mathrm{US}}}\int_0^{T_{\mathrm{US}}}R_{\mathrm{DA}}(r_{\mathrm{US}}(t))dt.$$

While estimating, relaxation time in the CDLR sub–system is assumed to be considerably less than T_{US} and

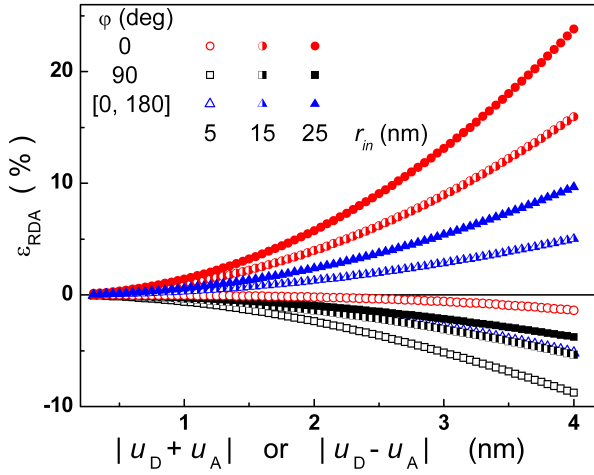FIG. 5. Simulated dependencies of AI changes of coupling parameter on the vibration amplitudes. Axis $|u_D + u_A|$ corresponds to $\delta = 0°$ case, whereas axis $|u_D + u_A|$ corresponds to $\delta = 180°$ case. The parameters are set to $a_0 = 3.23$ nm, $r_{in} = 5$ nm (open marks), 15 nm (semi–filled marks), and 25 nm (filled marks), $\varphi = 0°$ (circles), $90°$ (squares). Triangles correspond to mean ε_{RDA} value for $[0° \div 180°]$ φ range.

the previously used[41] value $a_0 = 3.23$ nm is utilized. Besides, the chosen u_D and u_A values are commensurate with u_{US}. But it is taken into account, that a displacement of the point defect without covalent bond could exceed a matrix atom displacement. At last, no US absorption by defect is assumed. In this simple case δ equals to $0°$, if $(\Delta\Omega_d^D \cdot \Delta\Omega_d^A) > 0$, or to $180°$, if $(\Delta\Omega_d^D \cdot \Delta\Omega_d^A) < 0$. In addition, ε_{RDA} dependence on u_D and u_A is only determined by $|u_D - u_A|$ ($\delta = 0°$ case) or $|u_D + u_A|$ ($\delta = 180°$ case). Moreover, these dependences are identical in both cases. The typical simulation results are shown in Fig. 5.

ε_σ depends on oscillation amplitudes with a similar features and does not depend on φ:

$$\varepsilon_\sigma = (u_D \pm u_A)^2 / 2\, r_{in}^2 = K_{US}^{DA} W_{US}, \qquad (15)$$

where "+" and "−" correspond to $\delta = 180°$ and $\delta = 0°$ respectively, K_{US}^{DA} characterizes defect couple–ultrasound interaction and depends on properties defects as well as crystal matrix. It is taken into account in Eq. (15), that $u_D, u_A \propto \xi_{US} \propto \sqrt{W_{US}}$.

Before analysing, it is worth keeping in mind, that CLDR current flows locally in the locations of extended defects.[41,58] On the other hand, dislocations are often situated in the SCR region perpendicularly to $p-n$ junction plane and investigated samples are not exception (see Section III C). If CDLR in the dislocation locations is assumed, then dislocations with edge component would influence on pair spatial orientation. Thus axis of donor–acceptor pair with $(\Delta\Omega_d^D \cdot \Delta\Omega_d^A > 0)$ should be predominantly situated parallel to a dislocation line, whereas pair of coupled defects with $(\Delta\Omega_d^D \cdot \Delta\Omega_d^A < 0)$ should be normal. As AW displacement is parallel to the $p-n$ junction plane, the most excited curiosity variants are following:

$\delta = 0°$, $\varphi = 90°$ ($\Delta\Omega_d^D \cdot \Delta\Omega_d^A > 0$ case);
$\delta = 180°$, $\varphi \in [0° \div 180°]$ ($\Delta\Omega_d^D \cdot \Delta\Omega_d^A < 0$ case).
In other words, all curves in Fig. 5 can be realized if defect volume relaxation of donor–like defect opposites in sign to that of acceptor–like defect. And only squares have to be under consideration in $\Delta\Omega_d^D \cdot \Delta\Omega_d^A > 0$ case.

In our opinion, taking into account experimental results and suggested model estimation:
(i) $E_{\tau g}$ and T_{id} are mainly determined by couple component energy levels. The alteration of $E_{\tau g}$ and T_{id} for nSC, g6SC, and g7SC in comparison with iSC testifies to change of defect (donor, acceptor, or both), which take part in CDLR, after irradiation. And g6SC defect is coincident to g7SC defect and differs from neutron–irradiated sample defect.
(ii) USL causes donor–acceptor distance change and results in ε_σ and ε_{RDA}, which increase with W_{US}.
(iii) Acoustically induced $E_{\tau g}$ (and T_{id}) modification, which is observed in g6SC, and g7SC only, testifies a rebuilding of γ–induced RD. I.e., γ–induced RD is conqurationally bistable (or metastable) and transform from ground state to another under US action. Similar AI defect variations were also reported previously.[3,5,32,59]
(iv) ε_σ sign is immutable — see Eq. (15), whereas ε_{RDA} sign can vary for pair with opposite relaxation volume component — see Fig. 5. Therefore Δn_{id} and $\varepsilon_{\tau g}$ sign change is evidence of transformation from $(\Delta\Omega_d^D \cdot \Delta\Omega_d^A > 0)$ to $(\Delta\Omega_d^D \cdot \Delta\Omega_d^A < 0)$ after irradiation. Transformation is confirmed by US influence efficiency rise in irradiated samples. Really, in the case of $(\Delta\Omega_d^D \cdot \Delta\Omega_d^A < 0)$ the US efficiency is determined by sum of pair component displacements, whereas in the contrary case — by difference. Conceivably, both donor and acceptor are interstitial–type at non–irradiated sample, and one of pair component is vacancy–type at irradiated samples. The defect configuration are discussed below, in Section III D.

B. Quasi–neutral region

Base lifetime mirrors the processes, which occur in the quasi–neutral region of p-n–structure. Fig. 6 shows the τ_n over the explored temperature range. Minority carrier lifetime expectedly rises with temperature increase and τ_n values equal to $2 \div 5$ μs for different samples at 320 K. These values correspond to $80 \div 130$ μm range of diffusion length. In our opinion, the observed τ_n dispersion is not defined by irradiation, but deals with sample–ancestor wafer inhomogeneity, which is revealed quite often.[60,61]

Really, the irradiation induced lifetime reduction is described by the Messenger-Spratt equation:[48]

$$\tau_n^{-1} = \tau_{n0}^{-1} + K_\tau \Psi, \qquad (16)$$

where τ_{n0} is the minority carrier lifetime in the non–irradiated sample, and K_τ is a lifetime damage–constants. The known K_τ values and estimated changes of reciprocal base lifetime $K_\tau \Psi$ are shown in Table V. One can see, that expected radiation–induced τ_n^{-1} change
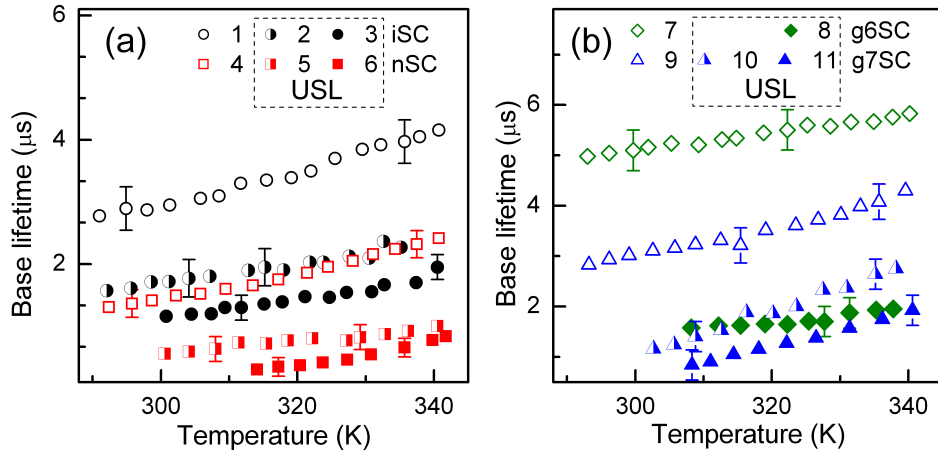
FIG. 6. Temperature dependences of base lifetime for non–irradiated (curves 1–3, circles), neutron–irradiated (4–6, squares) and γ–irradiated (7–11, diamonds and triangles) samples. The curves 1, 4, 7 and 9 (open marks) are obtained without USL, curves 2, 3, 5, 6, 8, 10, and 11 correspond to Ui–1, Ui–2, Un–1, Un–2, Ug6–2, Ug7–1, and Ug7–2 respectively.

TABLE V. Measured and estimated base lifetime parameters.

Sample	$\tau_{n,in}^{-1}$ (320 K) (10^5 s^{-1})	K_τ (cm^2/s)	$K_\tau \times \Psi$ (10^4 s^{-1})	K_{US}^{eff} (cm^2/W)
iSC	2.9	—	—	3.5
nSC	4.7	10^{-7}(Ref. 33) $2 \cdot 10^{-7}$(Ref. 62)	$4 \div 8$	7.1
g6SC	1.8	$5 \cdot 10^{-12}$	0.8	6.0
g7SC	2.8	(Refs. 33, 63)	8	5.2

equals to $(8 \div 17)$, 4, and 29 % of the measured value for samples nSC, g6SC, and g7SC respectively, and cannot explain the observed dispersion. Calculated lifetime changes $K_\tau \Psi$ are in quite good agreement with those, which are expected from RDs production — see Section III D.

Base lifetime can be expressed as following:[64]

$$\tau_n^{-1} = \tau_{bb}^{-1} + \tau_{CE\,Auger}^{-1} + \tau_{SRH}^{-1}, \qquad (17)$$

where τ_{bb}, $\tau_{CE\,Auger}$, τ_{SRH} are the lifetime due to band–to–band, Coloumb–enhanced Auger, and SRH recombination, respectively. Calculation shows, that $\tau_{bb}^{-1} = 14 \text{ s}^{-1}$, $\tau_{CE\,Auger}^{-1} = 6 \text{ s}^{-1}$, therefore τ_{SRH} should be under consideration only. In the cases of low injection level and single recombination centre, SRH lifetime is described by Eq. (10). If several centers are present, then

$$\tau_n^{-1} = \sum_i^{M_d} \tau_{n,i}^{-1} = \sum_i^{M_d} N_{d,i}, \sigma_{n,i}\, \upsilon_{th,n}, \qquad (18)$$

where M_d is total number of center, $\tau_{n,i}$ characterizes lifetime due to recombination by i–th defect, $N_{d,i}$ and $\sigma_{n,i}$ are concentration and electron CCS of i–th defect, recpectively.

Fig. 6 shows, that USL results in τ_n decrease. Relative AI changes of reciprocal base lifetime $\varepsilon_{\tau r} = (\tau_{n,in} -$

$\tau_{n,US})/\tau_{n,US}$ are listed in Table IV. As AI changes is reversible, in our opinion, this effect deals with increase of σ_n under US action. Following the empirical relation proposed by Ref. 65, we assume that Eq. (11) is correct for complex point defect too. But in this case, r is the distance between complex component. According to suggested in Section III A model, USL leads to r variation and σ_n change in line with Eq. (15). In case of CDLR, AI change of donor (or/and acceptor) SSC is supplemental to variation of both coupling parameter and couple distance. But this effect is a single for base lifetime.

On the other hand, every defect does not take part in AID effectively. If M_d^{AA} and M_d^{nonAA} are total numbers of acoustically active (AA) and non–AA center, then using Eq (18) base lifetime in sample without and with USL can be expressed as

$$\tau_{n,in}^{-1} = \sum_j^{M_d^{AA}} N_{d,j}, \sigma_{n,j}^{in}\, \upsilon_{th,n} + \sum_l^{M_d^{nonAA}} N_{d,l}, \sigma_{n,l}\, \upsilon_{th,n},$$

$$\tau_{n,US}^{-1} = \sum_j^{M_d^{AA}} N_{d,j}, \sigma_{n,j}^{US}\, \upsilon_{th,n} + \sum_l^{M_d^{nonAA}} N_{d,l}, \sigma_{n,l}\, \upsilon_{th,n}.$$

Using Eq (15), $\varepsilon_{\tau r}$ results in

$$\varepsilon_{\tau r} = K_{US}^{eff} W_{US}, \qquad (19)$$

where K_{US}^{eff} characterizes ADI in the sample and depends on concentration of both AA and non–AA centers

$$K_{US}^{eff} = \sum_j^{M_d^{AA}} \frac{\tau_{n,in}}{\tau_{n,j,in}} K_{US,j}, \qquad (20)$$

$K_{US,j}$ deals with j–th defect–ultrasound interaction.

The obtained dependences $\varepsilon_{\tau r}$ vs W_{US} are shown in Fig. 7. Dependences linearity is evidence of our assumption correctness. The determined K_{US}^{eff} values are listed in Table V. The non–monotonic K_{US}^{eff} alteration with γ dose is under consideration in Section III D.
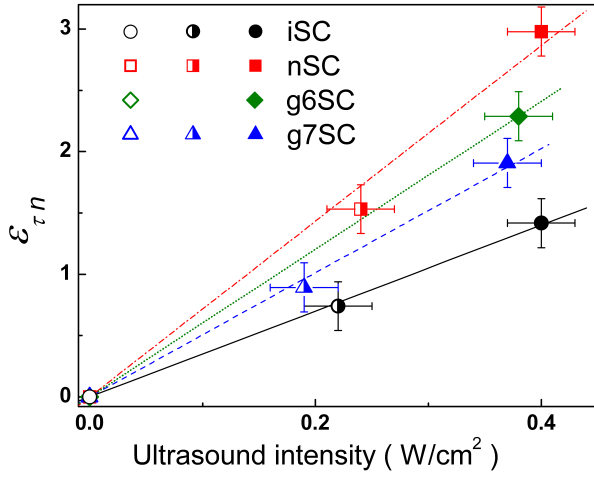
FIG. 7. Dependences of relative base lifetime change on US intensity for non–irradiated (circles), neutron–irradiated (squares), and γ–irradiated (triangles and diamonds) samples. Lines are the fitted curves using Eq. (19).

C. Shunt resistance

Fig. 8 shows the shunt resistance over the explored temperature range. One can see, that irradiation results in R_{sh} decrease. Besides the R_{sh} temperature dependence behavior is changed in γ–exposed samples. Namely the shunt resistance decreases with the temperature growth in iSC and nSC, whereas close to linear increase of R_{sh} vs T is observed in g6SC and g7SC at 293 K neighbourhood. We want to notice that R_{sh} axis is logarithmic and linear in Fig. 8(a) and Fig. 8(b), respectively.

Several non-mechanical reasons of p–n structure shunt resistance appearance are known.[66] They are aluminum particles, macroscopic Si_3N_4 inclusions, inversion layers at precipitates. So during firing Al will alloy in, leading to a p^+–doped region around the particle, which may compensate the emitter and may be in ohmic contact with the base. Inversion layers and Si_3N_4 inclusions occur in multicrystalline silicon cells mainly[66] and cannot cause a shunt resistance of investigated samples. In addition, dislocations, which intersect the junction, are generally held responsible as a possible source of ohmic current.[66–68] In our opinion, both aluminum particles and dislocations are present in the investigated structure. The overall shunt resistance can be expressed as

$$R_{sh}^{-1} = R_{sh,\mathrm{Al}}^{-1} + R_{sh,\mathrm{dis}}^{-1}, \qquad (21)$$

where $R_{sh,\mathrm{Al}}$ and $R_{sh,\mathrm{dis}}$ deal with aluminum particles and dislocations, respectively. The linear temperature dependence of metal particles $R_{sh,\mathrm{Al}}$ is suggested:

$$R_{sh,\mathrm{Al}} = R_{293,\mathrm{Al}}[1 + \alpha(T - 293)], \qquad (22)$$

where $R_{293,\mathrm{Al}}$ is the shunt resistance at 293 K and α is the resistance temperature coefficient.

Gopal and Gupta[42,43] introduced the model of dislocation–induced impedance of photovoltaic detector. According to this model, the $R_{sh,\mathrm{dis}}$ can be given by

$$R_{sh,\mathrm{dis}} = \frac{T}{\sigma_{\mathrm{dis}}} \left[\cosh\left(\frac{E_{\mathrm{dis}} - E_i}{kT} \right) + \cosh\left(\frac{U_s}{kT} \right) \right],$$
$$(23)$$

with

$$\sigma_{\mathrm{dis}} = \rho_{\mathrm{dis}} A q^2 A_{\mathrm{dis}} \sqrt{K_n K_p}\, N_{\mathrm{dis}}(n_p + p_p)/k, \qquad (24)$$

where E_{dis} is the energy level which significantly contributes to the dislocation recombination current, U_s is the potential at the surface of the dislocation core, ρ_{dis} and A_{dis} are the dislocation density and surface area, respectively, K_n and K_p are the capture probabilities for electrons and holes by the dislocation states, N_{dis} is the density of surface states at each dislocation. Eq. (23) is reduced for the simplified case of $K_p = K_n$.

α was determined from g7SC data. Obtained value $8.3 \cdot 10^{-3}$ K^{-1} is not far from resistance temperature coefficient of bulk Al ($4.3 \cdot 10^{-3}$ K^{-1}). Then we used Eqs. (21)–(23) to fit the experimental R_{sh} data. $R_{293,\mathrm{Al}}$, $(E_{\mathrm{dis}} - E_i)$, U_s, and σ_{dis} were taken as the fitting parameters. It was established that the good agreement of the experimental data with the fitting curves has been observed (see Fig. 8) for values $(E_{\mathrm{dis}} - E_i) = (0.46 \pm 0.02)$ eV and $U_s = (5 \pm 4) \times 10^{-8}$ eV, which were independent of irradiation and USL. The obtained $(E_{\mathrm{dis}} - E_i)$ corresponds to the carrier activation energy 0.10 ± 0.02 eV. This value is comparable to the activation energy of dislocation levels 0.08 eV, which was early reported[69–73] in Cz–Si:B too.[69–71]

Obtained $R_{293,\mathrm{Al}}$ and σ_{dis} are listed in Table III. $R_{293,\mathrm{Al}}$ does not depend on USL and increases with irradiation level. In our opinion, $R_{sh,\mathrm{dis}}$ is less than $R_{sh,\mathrm{Al}}$ in iSC. Irradiation leads to vacancy production and Al diffusion out of electrodes. As a result, Al particle quantity rises, $R_{sh,\mathrm{Al}}$ decreases and becomes key of overall shunt resistance value. The Al diffusion is more effective in γ–exposed samples due to more uniform distribution of irradiation–induced single vacancies.

σ_{dis} dispersion on sample set correlates to τ_n that. Hence it deals with wafer inhomogeneity too. USL leads to σ_{dis} increase, relative AI changes $\varepsilon_{\sigma\mathrm{dis}} = (\sigma_{\mathrm{dis,US}} - \sigma_{\mathrm{dis},in})/\sigma_{\mathrm{dis},in}$ are shown in Table IV. On our opinion this is caused by an A_{dis} augmentation. Namely, the dislocation core atom displacement is normal to the current direction. As the result, carriers are captured by dislocation levels from enlarged volume. Therefore the effective surface area increases and $LR_{sh,\mathrm{dis}}$ decreases under US action.

D. Defect type speculation

Lifetime killers in boron–doped Czochralski–grown Si are the boron–oxygen related (BO) defects,[74,75] iron–boron pairs[64,76,77] (or another Fe–related trap in the
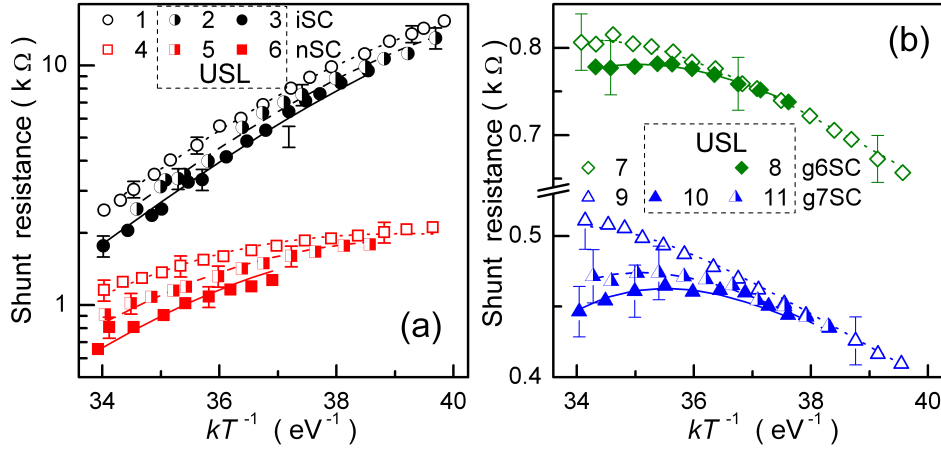
FIG. 8. Temperature dependences of shunt resistance for non–irradiated (curves 1–3, circles), neutron–irradiated (4–6, squares) and γ–irradiated (7–11, diamonds and triangles) samples. The curves 1, 4, 7 and 9 (open marks) are obtained without USL, curves 2, 3, 5, 6, 8, 10, and 11 correspond to Ui–1, Ui–2, Un–1, Un–2, Ug6–2, Ug7–1, and Ug7–2 respectively. The marks are the experimental results, the lines are the fitted curves using Eq. (21)-(23).

n^+p–junctions[78,79]), and oxide precipitates.[60,61,64,80–82] The first two defects are sensitive to an intensive illumination at room temperature. To determine the major recombination center of investigated samples the following experimental procedure has been used. The non-irradiated sample was light soaked under halogen lamp (2 Suns) illumination at approximately 305 K. The illumination varied from 1 h to 8 h. After illumination sample is stored in the dark at room temperature. To determine the parameters kinetics I–V characteristics have been measured with interval 10–15 min at room temperature over a period 5 h after illumination stopping. To determine the permanent light–induced change the I–V characteristics have been measured in 48 h after illumination. After accumulated time under illumination had run up to 15 h the iSC was annealed at 200 °C for 10 min in the dark and parameters were determined at room temperature. After that, the illumination and measurements were repeated.

In order to keep the volume of this paper at an rather reasonable size, the detailed results are not shown. But main result are following. Illumination did not result in permanent change of either of τ_g, τ_n, n_{id} before as well as after annealing. Therefore BO influence on recombination in both SCR and base can be neglected. n_{id} increase (about 0.03) and τ_g decrease (about 10 %) were observed after illumination immediately. These changes vanished gradually, both n_{id} and τ_g time dependences were very similar to those, which is expected[77] for Fe_iB_s repairing. Hence iron–boron pairs take part in SCR recombination. On the other hand, electron and hole CCS of released by illumination interstitial iron are 1.7 and 0.04 times[77] as much as those of Fe_iB_s. A small (about 10 %) τ_g alteration, which is caused by light, is evidence of supporting role of iron–boron pair in SCR recombination. Furthermore, since τ_n does not depend on illumination, then Fe_iB_s has not an influence on base lifetime.

As a result, oxide precipitates are number one in SCR and base recombination. According to Murphy et al.[80,81], at least two independent oxide precipitate related defects are exist. These defects have $\sigma_n/\sigma_p = 157$ and $\sigma_p/\sigma_n = 1200$ respectively.[81] So, they are suitable to CDLR. On the basis of mentioned above, we conclude that the defect, which responsible for AI phenomena in nSC, is oxide precipitate mainly.

It is worth keeping doping level, oxygen concentration and dose in mind when RD type is foreseen. In our case (Czochralski, oxygen–rich, $\sim 7 \cdot 10^{17}$ cm^{-3}, p–Si with boron concentration $\sim 10^{15}$ cm^{-3} and low dose) it is expected, that C_iO_i, vacancy clusters V_n (divacancy V_2, trivacancy V_3, ...) and VO_i are produced mainly by neutron irradiation[83–85] and C_iO_i and VO_i by γ–rays.[85–88] The RD concentration $N_{t,RD}$ is proportionate to dose, the known introduction rate for neutron η_n and gamma η_γ irradiation in Cz–Si are shown in Table VI. The expected $N_{t,RD}$ for investigated samples are listed in Table VI too.

Another defects, which can be created by irradiation in silicon, are I_p–center, bistable donor (BD), B_iO_i and C_iC_s. But first and second defects are characterized by small introduction rate. For example, BD expected[84,92] concentration is only $(1 \div 2) \cdot 10^{10}$ cm^{-3} in nSC and g7SC. B_iO_i lack in investigated samples deals with low boron concentration[93]. Lastly, C_iC_s creation is suppressed in oxygen–rich crystal.[83,86,87] Besides C_iC_s is not recombination active center.[94]

To estimate RD influence on base lifetime, one can use Eq. (18) and takes into account, that VO_i is not active recombination center in p–Si.[63,95–98] Estimated $\tau_{n,RD}$ for C_iO_i, V_2, and V_3 are shown in Table VI. One can recognize, that τ_n effected mainly by C_iO_i and vacancy clusters in γ– and neutron–irradiated samples, respectively. We want to note, that nSc, g6Sc, g7SC sums of $\tau_{n,RD}$ are in quite good agreement with $(K_\tau \cdot \Psi)$ values.

Lets pay attention to K_{US}^{eff} and assume, that $M_d^{AA} = 1$,

TABLE VI. Cited and calculated defect parameters.

Defect	σ_n (10^{-15} cm^2)	η_n (cm^{-1}) Ref. 85	η_γ	$N_{t,\mathrm{RD}}$(10^{11} cm^{-3})			$\tau_{n,\mathrm{RD}}^{-1}$ (10^4 s^{-1})		
				nSC	g6SC	g7SC	nSC	g6SC	g7SC
C_iO_i	0.7 (Ref. 86) 0.9 (Ref. 87)	1.38	$6 \cdot 10^5$ rad^{-1}cm^{-3} (Ref. 86) $4 \cdot 10^{-4}$ cm^{-1} (Ref. 87)	5.5	6	60	$0.8 \div 1$	$0.9 \div 1.1$	$9 \div 11$
V_2	3 (Ref. 86) 2 (Ref. 89)	1.21	$3 \cdot 10^4$ rad^{-1}cm^{-3} (Ref. 86)	4.8	0.3	3	$2.2 \div 3.3$	$0.1 \div 0.2$	$1 \div 2$
V_3	2.4 (Ref. 90)	0.37	—	1.5	—	—	0.7	—	—
VO_i	2.4 (Ref. 88) 4 (Ref. 91)	0.52	$7 \cdot 10^5$ rad^{-1}cm^{-3} (Ref. 86) $4 \cdot 10^{-4}$ cm^{-1} (Ref. 87)	2	$6 \div 7$	$60 \div 70$			

$M_d^{\mathtt{nonAA}} = 1$ in non–irradiated sample and US interaction with C_iO_i and V_n is described by $K_{\mathtt{US}}^{\mathtt{CO}}$ and $K_{\mathtt{US}}^{\mathtt{V}}$, respectively. Using Eq. (20), $K_{\mathtt{US}}^{\mathtt{eff}}$ for nSC and irradiated samples can be expressed as

$K_{\mathtt{US}}^{\mathtt{eff}} = K_{\mathtt{US}}^{\mathtt{AA}} \tau_{n,in}/\tau_{n,in}^{\mathtt{AA}}$,

$K_{\mathtt{US}}^{\mathtt{eff}} = K_{\mathtt{US}}^{\mathtt{AA}} \tau_{n,in}/\tau_{n,in}^{\mathtt{AA}} + K_{\mathtt{US}}^{\mathtt{CO}} \tau_{n,in}/\tau_{n,\mathrm{RD}}^{\mathtt{CO}} + K_{\mathtt{US}}^{\mathtt{V}} \tau_{n,in}/\tau_{n,\mathrm{RD}}^{\mathtt{V}}$,

where $\tau_{n,in}^{\mathtt{AA}}$ is the base lifetime in case of non-radiative AA defect with $K_{\mathtt{US}}^{\mathtt{AA}}$ is only present in sample.

Two extreme cases are opportune to analysis. In the first one, non–AA defects are distributed uniformly across wafer and AA defects define a distinction of $(\tau_{n,in}^{-1} - K_\tau \cdot \Psi)$ value for different samples. In the second one, a non–AA defect distribution is not uniform, whereas $\tau_{n,in}^{\mathtt{AA}}$ is identical for iSC, nSC, g6SC, and g7SC. However, in the first case (as well as in case of $M_d^{\mathtt{nonAA}} = 0$), experimental $K_{\mathtt{US}}^{\mathtt{eff}}$ values lead to unreal (negative) values of $K_{\mathtt{US,j}}$. In the second case, using Eq. (20) and data of Tables V and VI, the following equation array can be written:

iSC : $3.5 = K_{\mathtt{US}}^{\mathtt{AA}} \cdot (\tau_{n,in}^{\mathtt{AA}})^{-1} /2.9$,

nSC : $7.1 = K_{\mathtt{US}}^{\mathtt{AA}} \cdot (\tau_{n,in}^{\mathtt{AA}})^{-1} /4.7 + 0.09 \, K_{\mathtt{US}}^{\mathtt{V}} + 0.02 \, K_{\mathtt{US}}^{\mathtt{CO}}$,

g6SC : $6.0 = K_{\mathtt{US}}^{\mathtt{AA}} \cdot (\tau_{n,in}^{\mathtt{AA}})^{-1} /1.8 + 0.01 \, K_{\mathtt{US}}^{\mathtt{V}} + 0.05 \, K_{\mathtt{US}}^{\mathtt{CO}}$,

g7SC : $5.2 = K_{\mathtt{US}}^{\mathtt{AA}} \cdot (\tau_{n,in}^{\mathtt{AA}})^{-1} /2.8 + 0.05 \, K_{\mathtt{US}}^{\mathtt{V}} + 0.35 \, K_{\mathtt{US}}^{\mathtt{CO}}$,

where $(\tau_{n,in}^{\mathtt{AA}})^{-1}$ in $10^4/$ s. These equations are correct if $K_{\mathtt{US}}^{\mathtt{AA}} \cdot (\tau_{n,in}^{\mathtt{AA}})^{-1} = (10 \pm 3)$ cm^2/W, $K_{\mathtt{US}}^{\mathtt{V}} = (42 \pm 15)$ cm^2/W, $K_{\mathtt{US}}^{\mathtt{CO}} = 0$. Since $(\tau_{n,in}^{\mathtt{AA}})^{-1} < 1.83$, then $K_{\mathtt{US}}^{\mathtt{AA}} > 5$ cm^2/W. Thus observed base lifetime change is caused by AI modification of the same defect (most likely oxide precipitates) in both non–irradiated and γ–irradiated samples. This effect is added by AI divacancy alteration in neutron–irradiated samples. In other words, C_iO_i is non–AA defect, whereas V_2 is AA defect.

As to SCR recombination, in our judgement, τ_g and n_{id} in non–irradiated sample are affected by modification of coupled oxide precipitate related defects under US action. As assumed above in Section III A, the AA radiation defects with $\Delta\Omega_d < 0$ take part in CDLR in irradiated samples. Divacancy is quite suitable for AI influence on τ_g and n_{id} in nSC. But a bistable (or metastable) defect is expected in γ–irradiated samples. There are known a few such defect with $\Delta\Omega_d < 0$ in Si, viz VO_2,[99] V_3,[90] and

VO_i.[100] VO_2 appears after 300°C annealing of irradiated crystal, V_3 is not typical defect for $\gamma-^{60}$Co exposed silicon. On the other hand, VO_i is largo manum produced and can take part in CDLR around n^+–p interface in g6SC and g7SC. Metastable state, which is commonly observed at low temperature, differs by large distance between oxygen and vacancy and by more deep energy level.[100] The volume change of entire complex is negative, whereas for complex component $\Delta\Omega_d(V) < 0$ and $\Delta\Omega_d(O_i) > 0$. Hence, under assumption, VO_i is favorable pair for AI alteration of component distance. Thus VO_i can be rebuild to metastable configuration by USL and this effect results in both T_{id} and $E_{\tau g}$ change.

IV. CONCLUSION

The experimental investigation of ultrasound influence on the I–V characteristic of silicon n^+–p–structure has been carried out. The effects of reactor neutrons and ^{60}Co gamma radiation on ultrasound influence were studied. The investigation has revealed the acoustically driven reversible decrease of both minority carrier lifetime in structure base and shunt resistance. The effect intensifies in irradiated structures. The analysis has shown that the acoustically induced increase of carrier capture coefficient of point or extended defects is a reason of observed effects. It has been found out that the ultrasound loading leads to the reversible modification of SCR carrier lifetime and ideality factor. Changes are opposite in sign in non–irradiated and irradiated structures. The qualitative model of observed phenomenon, which is based on the increase of a distance between coupled defects or between defect complex components under ultrasound action, has been under consideration. It has been shown that divacancy and pair vacancy–interstitial oxygen are effectively modified by ultrasound in neutron– and γ–exposed structures respectively. Complex interstitial carbon–interstitial oxygen does not practically take part in acousto–defect interaction. Thus, ultrasound can be an effective tool for controlling silicon structure characteristics.

[1]M. Jivanescu, A. Romanyuk, and A. Stesmans, J. Appl. Phys. **107**, 114307 (2010).

[2] A. Romanyuk, P. Oelhafen, R. Kurps, and V. Melnik, Appl. Phys. Lett. **90**, 013118 (2007).

[3] I. A. Buyanova, S. S. Ostapenko, M. K. Sheinkman, and M. Murrikov, Semicond. Sci. Technol. **9**, 158 (1994).

[4] O. Korotchenkov and H. Grimmliss, Phys. Rev. B **52**, 14598 (1995).

[5] O. Y. Olikh, Semiconductors **43**, 745 (2009).

[6] S. S. Ostapenko and R. E. Bell, Journal of Applied Physics **77**, 5458 (1995).

[7] I. Ostrovskii, O. Korotchenkov, O. Olikh, A. Podolyan, R. Chupryna, and M. Torres-Cisneros, J. Opt. A: Pure Appl. Opt. **3**, S82 (2001).

[8] D. Kropman, V. Seeman, S. Dolgov, and A. Medvids, phys. stat. sol. (c) **13**, 793 (2016).

[9] N. Zaveryukhina, E. Zaveryukhina, S. Vlasov, and B. Zaveryukhin, Technical Physics Letters **34**, 241 (2008).

[10] S. A. Mirsagatov, I. B. Sapaeva, and Z. Nazarov, Inorganic Materials **51**, 1 (2015).

[11] R. Savkina, A. Smirnov, T. Kryshtab, and A. Kryvko, Mater. Sci. Semicond. Process. **37**, 179 (2015).

[12] M. Virot, R. Pflieger, E. V. Skorb, J. Ravaux, T. Zemb, and H. Mohwald, J. Phys. Chem. C **119**, 15493 (2012).

[13] O. Y. Olikh, K. V. Voytenko, R. M. Burbelo, and J. M. Olikh, Journal of Semiconductors **37**, 122002 (2016).

[14] O. Olikh, Semiconductors **45**, 798 (2011).

[15] A. Davletova and S. Z. Karazhanov, Journal of Physics and Chemistry of Solids **70**, 989 (2009).

[16] A. Davletova and S. Z. Karazhanov, Journal of Physics D: Applied Physics **41**, 165107 (2008).

[17] V. Melnik, Y. Olikh, V. Popov, B. Romanyuk, Y. Goltvyanskii, and A. Evtukh, Materials Science & Engineering, B: Solid-State Materials for Advanced Technology **124–125**, 327 (2005).

[18] O. Y. Olikh, K. V. Voytenko, and R. M. Burbelo, Journal of Applied Physics **117**, 044505 (2015).

[19] O. Olikh, Ultrasonics **56**, 545 (2015).

[20] V. N. Pavlovich, phys. stat. sol. (b) **180**, 97 (1993).

[21] F. Mirzade, J. Appl. Phys. **110**, 064906 (2011).

[22] R. Peleshchak, O. Kuzyk, and O. Dan'kiv, Ukr. J. Phys. **61**, 741 (2016).

[23] V. D. Krevchik, R. A. Muminov, and A. Y. Yafasov, phys. stat. sol. (a) **63**, K159 (1981).

[24] F. Mirzade, J. Appl. Phys. **97**, 084911 (2005).

[25] I. Ostrovskii and O. Korotchenkov, Solid State Commun. **82**, 267 (1992).

[26] O. Olikh and K. Voytenko, Ultrasonics **66**, 1 (2016).

[27] N. Guseynov, Y. Olikh, and S. Askerov, Tech. Phys. Lett. **33**, 18 (2007).

[28] P. Parchinskii, S. Vlasov, and L. Ligai, Semiconductors **40**, 808 (2006).

[29] A. Gorb, O. Korotchenkov, O. Olikh, and A. Podolian, IEEE Trans. Nucl. Sci. **57**, 1632 (2010).

[30] A. O. Podolian, A. B. Nadtochiy, and O. A. Korotchenkov, Tech. Phys. Lett. **38**, 405 (2012).

[31] Y. Olikh, M. Tymochko, and A. Dolgolenko, Tech. Phys. Lett. **32**, 586 (2006).

[32] Y. Olikh and M. Tymochko, Tech. Phys. Lett. **37**, 37 (2011).

[33] H. Jafari and S. Feghhi, Nucl. Instrum. Methods Phys. Res., Sect. A **816**, 62 (2016).

[34] Y. P. Rao, K. Praveen, Y. R. Rani, A. Tripathi, and A. G. Prakash, Nucl. Instrum. Methods Phys. Res., Sect. B **316**, 205 (2013).

[35] M. Moll, H. Feick, E. Fretwurst, G. Lindström, and C. Schütze, Nucl. Instrum. Methods Phys. Res., Sect. A **388**, 335 (1997).

[36] J. Srour, C. Marshall, and P. Marshall, IEEE Trans. Nucl. Sci. **50**, 653 (2003).

[37] I. Pintilie, G. Lindstroem, A. Junkes, and E. Fretwurst, Nucl. Instrum. Methods Phys. Res., Sect. A **611**, 52 (2009).

[38] N. Arutyunov, N. Bennett, N. Wight, R. Krause-Rehberg, V. Emtsev, N. Abrosimov, and V. Kozlovski, phys. stat. sol. (b) **253**, 2175 (2016).

[39] C. A. Londos, G. Antonaras, and A. Chroneos, J. Appl. Phys. **114**, 193513 (2013).

[40] A. Schenka and U. Krumbein, Journal of Applied Physics **78**, 3185 (1995).

[41] S. Steingrube, O. Breitenstein, K. Ramspeck, S. Glunz, A. Schenk, and P. P. Altermatt, Journal of Applied Physics **110**, 014515 (2011).

[42] V. Gopal and S. Gupta, IEEE Trans. Electron Devices **50**, 1220 (2003).

[43] V. Gopal and S. Gupta, IEEE Trans. Electron Devices **51**, 1078 (2004).

[44] A. Akkerman, J. Barak, M. Chadwick, J. Levinson, M. Murat, and Y. Lifshitz, Radiat Phys Chem **62**, 301 (2001).

[45] D. Bräunig and F. Wulf, Radiat. Phys. Chem. **43**, 105 (1994).

[46] A. B. Sproul and M. A. Green, J. Appl. Phys. **73**, 1214 (1993).

[47] D. K. Schroder, *Semiconductor Material and Device Characterization*, 3rd ed. (John Wiley & Sons, New Jersey, 2006).

[48] A. McEvoy, T. Markvart, and L. Castaner, eds., *Solar Cells. Materials, Manufacture and Operation*, 2nd ed. (Academic Press, Oxford, 2013).

[49] K. Wang and M. Ye, Solid-State Electron. **53**, 234 (2009).

[50] D. Schroder, IEEE Trans. Electron Devices **29**, 1336 (1982).

[51] H. Aharoni, T. Ohmi, M. M. Oka, A. Nakada, and Y. Tamai, J. Appl. Phys. **81**, 1270 (1997).

[52] A. S. H. van der Heide, A. Schonecker, J. H. Bultman, and W. C. Sinke, Progress in Photovoltaics: Research and Applications **13**, 3 (2005).

[53] J. Beier and B. Voss, in *Proceedings of the 23rd IEEE Photovoltaic Specialists Conference* (1993) pp. 321–326, Louisville, KY, USA.

[54] J. M. Shah, Y.-L. Li, T. Gessmann, and E. F. Schubert, J. Appl. Phys. **94**, 2627 (2003).

[55] A. Kaminski, J. J. Marchand, H. E. Omari, A. Laugier, Q. N. Le, and D. Sarti, in *Proceedings of the 25th IEEE Photovoltaic Specialists Conference* (1996) pp. 573–576, Washington, DC, USA.

[56] W. M. Chen, B. Monemar, E. Janzén, and J. L. Lindström, Phys. Rev. Lett. **67**, 1914 (1991).

[57] A. M. Frens, M. T. Bennebroek, A. Zakrzewski, J. Schmidt, W. M. Chen, E. Janzén, J. L. Lindström, and B. Monemar, Phys. Rev. Lett. **72**, 2939 (1994).

[58] O. Breitenstein, J. Bauer, P. P. Altermatt, and K. Ramspeck, Solid State Phenomena **156–158**, 1 (2010).

[59] T. Wosinski, A. Makosa, and Z. Witczak, Semicond. Sci. Technol. **9**, 2047 (1994).

[60] L. Chen, X. Yu, P. Chen, P. Wang, X. Gu, J. Lu, and D. Yang, Sol. Energy Mater. Sol. Cells **95**, 3148 (2011).

[61] J. Schön, A. Youssef, S. Park, L. E. Mundt, T. Niewelt, S. Mack, K. Nakajima, K. Morishita, R. Murai, M. A. Jensen, T. Buonassisi, and M. C. Schubert, J. Appl. Phys. **120**, 105703 (2016).

[62] E. Gaubas, A. Uleckas, and J. Vaitkus, Nucl. Instrum. Methods Phys. Res., Sect. A **607**, 92 (2009).

[63] I. I. Kolkovskii, P. F. Lugakov, and V. V. Shusha, phys. stat. sol. (a) **83**, 299 (1984).

[64] J. D. Murphy, K. Bothe, M. Olmo, V. V. Voronkov, and R. J. Falster, J. Appl. Phys. **110**, 053713 (2011).

[65] D. G. Thomas, J. Hopfield, and W. M. Augistyniak, Phys. Rev. **140**, A202 (1965).

[66] O. Breitenstein, J. P. Rakotoniaina, M. H. Al Rifai, and M. Werner, Progress in Photovoltaics: Research and Applications **12**, 529 (2004).

[67] V. Gopal, J. Appl. Phys. **116**, 084502 (2014).

[68] I. Baker and C. Maxey, J. Electron. Mater. **30**, 682 (2001).

[69] A. Castaldini, D. Cavalcoli, A. Cavallini, and S. Pizzini, Phys. Rev. Lett. **95**, 076401 (2005).

[70] I. Isakova, A. Bondarenko, O. Vyvenko, V. Vdovin, E. Ubyivovk, and O. Kononchuk, Journal of Physics: Conference Series **281**, 012010 (2011).

[71] X. Yu, O. Vyvenko, M. Kittler, W. Seifert, T. Mtchedlidze, T. Arguirov, and M. Reiche, Semiconductors **41**, 458 (2007).

[72] V. Kveder, M. Kittler, and W. Schröter, Phys. Rev. B **63**, 115208 (2001).

[73] M. Trushin, O. Vyvenko, T. Mchedlidze, O. Kononchuk, and M. Kittler, Solid State Phenomena **156–158**, 283 (2010).

[74] J. Lindroos and H. Savin, Sol. Energy Mater. Sol. Cells **147**, 115 (2016).

[75] T. Niewelt, J. Schöon, W. Warta, S. W. Glunz, and M. C. Schubert, IEEE Journal of Photovoltaics **7**, 383 (2017).

[76] V. Vahanissi, A. Haarahiltunen, H. Talvitie, M. Yli-Koski, and H. Savin, Progress in Photovoltaics: Research and Applications **21**, 1127 (2012).

[77] J. Schmidt, Progress in Photovoltaics: Research and Applications **13**, 325 (2005).

[78] T. Mchedlidze and J. Weber, phys. stat. sol. (b) **251**, 1608 (2014).

[79] T. Mchedlidze, L. Scheffler, J. Weber, M. Herms, J. Neusel, V. Osinniy, C. Moller, and K. Lauer, J. Appl. Phys. **103**, 013901 (2013).

[80] J. Murphy, J. McGuire, K. Bothe, V. Voronkov, and R. Falster, Sol. Energy Mater. Sol. Cells **120**, 402 (2014).

[81] J. D. Murphy, K. Bothe, R. Krain, V. V. Voronkov, and R. J. Falster, J. Appl. Phys. **111**, 113709 (2012).

[82] M. Porrini and P. Tessariol, Materials Science and Engineering B **73**, 244 (2000).

[83] G. Lindström, M. Ahmed, S. Albergo, P. Allport, D. Anderson, L. Andricek, M. Angarano, V. Augelli, N. Bacchetta, P. Bartalini, R. Bates, U. Biggeri, G. Bilei, D. Bisello, D. Boemi, E. Borchi, T. Botila, T. Brodbeck, M. Bruzzi, T. Budzynski, P. Burger, F. Campabadal, G. Casse, E. Catacchini, A. Chilingarov, P. Ciampolini, V. Cindro, M. Costa, D. Creanza, P. Clauws, C. Da Via, G. Davies, W. De Boer, R. DellOrso, M. De Palma, B. Dezillie, V. Eremin, O. Evrard, G. Fallica, G. Fanouraki, H. Feick, E. Focardi, L. Fonseca, E. Fretwurst, J. Fuster, K. Gabathuler, M. Glaser, P. Grabiec, E. Grigorievt, G. Hall, M. Hanlond, F. Hauler, S. Heising, A. , Holmes-Siedle, R. Horisberger, G. Hughes, M. Huhtinen, I. Ilyashenko, A. Ivanov, B. Jones, L. Jungermann, A. Kaminsky, Z. Kohout, G. Kramberger, M. Kuhnke, S. Kwan, F. Lemeilleur, C. Leroy, M. Letheren, Z. Li, T. Ligonzo, V. Linhart, P. Litovchenko, D. Loukas, M. Lozano, Z. Luczynski, G. Lutz, G. MacEvoy, S. Manolopoulos, A. Markou, C. Martinez, A. Messineo, M. Mikuž, M. Moll, E. Nossarzewska, G. Ottaviani, V. Oshea, G. Parrini, D. Passeri, D. Petre, A. Pickford, I. Pintilie, L. Pintilie, S. Pospisil, R. Potenza, C. Raine, J. Rafi, P. Ratoff, H. Richter, P. Riedler, S. Roe, P. Roy, A. Ruzin, A. Ryazanov, A. Santocchia, L. Schiavulli, P. Sicho, I. Siotis, T. Sloan, W. Slysz, K. Smith, M. Solanky, B. Sopko, S. K., B. Sundby Avset, S. B., C. Tivarus, G. Tonelli, A. Tricomi, S. Tzamarias, G. Valvo, A. Vasilescu, A. Vayaki, E. Verbitskaya, P. Verdini, V. Vrba, S. Watts, E. Weber, M. Wegrzecki, I. Wegrzecka, P. Weilhammer, R. Wheadon, C. Wilburn, I. Wilhelm, R. Wunstorf, J. Wüstenfeld, J. Wyss, K. Zankel, P. Zabierowski, and D. Žontar, Nucl. Instrum. Methods Phys. Res., Sect. A **406**, 308 (2001).

[84] I. Pintilie, G. Lindstroem, A. Junkes, and E. Fretwurst, Nucl. Instrum. Methods Phys. Res., Sect. A **611**, 52 (2009).

[85] M. Moll, *Radiation damage in silicon particle detectors: Microscopic defects and macroscopic properties*, Ph.D. thesis, Universität Hamburg (1999).

[86] J. Stahl, E. Fretwurst, G. Lindström, and I. Pintilie, Nucl. Instrum. Methods Phys. Res., Sect. A **512**, 111 (2003).

[87] I. I. Kolkovskii and V. Lukyanitsa, Semiconductors **31**, 340 (1997).

[88] R. Siemieniec, W. Sudkamp, and J. Lutz, in *Proceedings of the Fourth IEEE International Caracas Conference on Devices, Circuits and Systems* (Oranjestad, Aruba, Netherlands, 2002) pp. D029–1–D029–6.

[89] S. D. Brotherton and P. Bradley, J. Appl. Phys. **53**, 5720 (1982).

[90] V. P. Markevich, A. R. Peaker, S. B. Lastovskii, L. I. Murin, J. Coutinho, V. J. B. Torres, P. R. Briddon, L. Dobaczewski, E. V. Monakhov, and B. G. Svensson, Phys. Rev. B **80**, 235207 (2009).

[91] H. Bleichner, P. Jonsson, N. Keskitalo, and E. Nordlander, J. Appl. Phys. **79**, 9142 (1996).

[92] E. Fretwurst, F. Hönniger, G. Kramberger, G. Lindström, I. Pintilie, and R. Röder, Nucl. Instrum. Methods Phys. Res., Sect. A **583**, 58 (2007).

[93] L. C. Kimerling, M. Asom, J. Benton, P. Drevinsky, and C. Caefer, Materials Science Forum **38–41**, 141 (1989).

[94] L. W. Song, X. D. Zhan, B. W. Benson, and G. D. Watkins, Phys. Rev. B **42**, 5765 (1990).

[95] J. L. Benton, S. Libertino, P. Kringhøj, D. J. Eaglesham, J. M. Poate, and S. Coffa, J. Appl. Phys. **82**, 120 (1997).

[96] S. Coffa, V. Privitera, F. Priolo, S. Libertino, and G. Mannino, J. Appl. Phys. **81**, 1639 (1997).

[97] N. Ganagona, B. Raeissi, L. Vines, E. V. Monakhov, and B. G. Svensson, phys. stat. sol. (c) **9**, 2009 (2012).

[98] L. Vines, E. V. Monakhov, A. Y. Kuznetsov, R. Kozłowski, P. Kaminski, and B. G. Svensson, Phys. Rev. B **78**, 085205 (2008).

[99] L. I. Murin, V. P. Markevich, I. F. Medvedeva, and L. Dobaczewski, Semiconductors **40**, 1282 (2006).

[100] B. N. Mukashev, K. A. Abdullin, and Y. V. Gorelkinskii, Physics–Uspekhi **43**, 139 (2000).